Archives of Biochemistry and Biophysics 758 (2024) 110074

Contents lists available at ScienceDirect

Archives of Biochemistry and Biophysics

journal homepage: www.elsevier.com/locate/yabbi

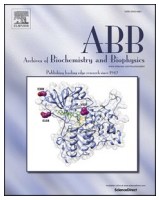

Comparative CO_2 and SiO_2 hydratase activity of an enzyme from the siliceous demosponge *Suberites domuncula*

Andrea Angeli [a], Viviana De Luca [b], Clemente Capasso [b,**], Luigi F. Di Costanzo [c,*], Claudiu T. Supuran [a]

[a] NEUROFARBA Department, Sezione di Scienze Farmaceutiche, University of Florence, Via Ugo Schiff 6, 50019, Sesto Fiorentino, Florence, Italy
[b] Department of Biology, Agriculture and Food Sciences, Institute of Biosciences and Bioresources, CNR, Via Pietro Castellino 111, 80131, Napoli, Italy
[c] Department of Agriculture, University of Napoli Federico II, Via Università 100, 80055, Portici, NA, Italy

ARTICLE INFO

Keywords:
Silicase
Silica degradation
Carbonic anhydrase
Versatile catalytic action

ABSTRACT

Silicase, an enzyme that catalyzes the hydrolysis of silicon-oxygen bonds, is a crucial player in breaking down silicates into silicic acid, particularly in organisms like aquatic sponges with siliceous skeletons. Despite its significance, our understanding of silicase remains limited. This study comprehensively examines silicase from the demosponge *Suberites domuncula*, focusing on its kinetics toward CO_2 as a substrate, as well as its silicase and esterase activity. It investigates inhibition and activation profiles with a range of inhibitors and activators belonging to various classes. By comparing its esterase activity to human carbonic anhydrase II, we gain insights into its enzymatic properties. Moreover, we investigate silicase's inhibition and activation profiles, providing valuable information for potential applications. We explore the evolutionary relationship of silicase with related enzymes, revealing potential functional roles in biological systems. Additionally, we propose a biochemical mechanism through three-dimensional modeling, shedding light on its catalytic mechanisms and structural features for both silicase activity and CO_2 hydration. We highlight nature's utilization of enzymatic expertise in silica metabolism. This study enhances our understanding of silicase and contributes to broader insights into ecosystem functioning and Earth's geochemical cycles, emphasizing the intricate interplay between biology and the environment.

1. Introduction

Silicase catalyzes the hydrolysis of silicon-oxygen bonds, breaking down silicates into silicic acid, a process of significant interest due to its rarity in biological systems [1]. This enzyme plays a pivotal role in silicon metabolism within plants and diatoms, holding significant importance across various biological processes, including growth, disease defense, and response to environmental stress [2]. Many sponges are characterized by an internal skeleton composed of spicules made primarily of silicon dioxide (silica) and calcium carbonate. These sponges rely on silicase enzymes to break down and remodel their rigid structures [3,4]. These siliceous organisms possess the remarkable ability to rapidly grow exoskeletal structures, such as frustules and spicules [5]. The enzymatic activity of silicase contributes to the breakdown of silicon dioxide, a material ubiquitous and highly abundant among oxides in the Earth's crust [6]. It's widely acknowledged that silicate-based minerals constitute over 90 % of all known terrestrial minerals [7]. Silicate minerals are initially incorporated into biogenic silica by organisms such as diatoms and sponges [8]. This biogenic silica then undergoes biological weathering, initiated by organisms like lichens and plants, releasing silicic acid that gradually dissolves silicate minerals. Sponges, along with diatoms and other single-celled organisms, contribute to the sedimentation of biogenic silica, transporting it to the ocean depths. This occurs through a phenomenon recognized as the biological pump, as shown in Scheme 1 [9–11]. Upon death or decay of sponges, silica stored in their tissues can be released back into the soil or water, contributing to the recycling of silicates. Therefore, these organisms play a crucial role both in the carbon and silicon cycles by consuming CO_2 dissolved in marine water, highlighting the interconnectedness of the carbon and silicon biochemical cycles (see Scheme 1) [12–14].

Silicon, essential for both plant and animal life, provides structural support in plants and serves as a defense mechanism against herbivores

* Corresponding author.
** Corresponding author.
E-mail addresses: clemente.capasso@ibbr.cnr.it (C. Capasso), luigi.dicostanzo4@unina.it (L.F. Di Costanzo).

https://doi.org/10.1016/j.abb.2024.110074
Received 11 May 2024; Received in revised form 19 June 2024; Accepted 22 June 2024
Available online 25 June 2024

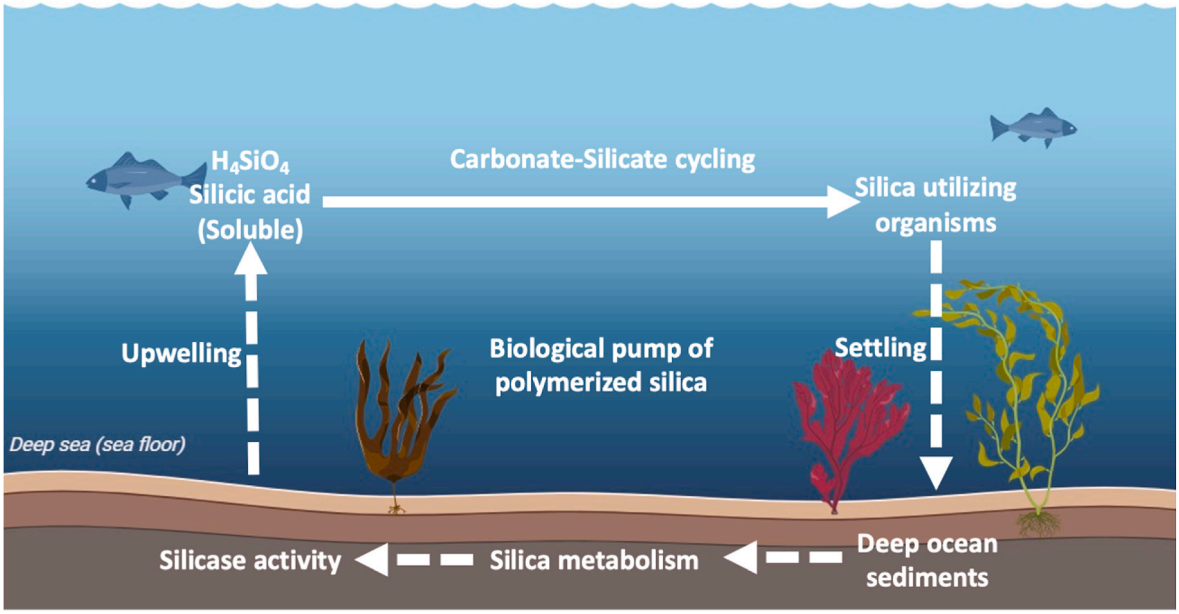

Scheme 1. Interconnection between carbonate and silicate cycles. Organisms utilize silica, which settles in deep oceanic sediments. Polymerized silica enters silica metabolism, where silicase plays a crucial role in its decomposition. Subsequently, enzymatically soluble silicic acid re-enters the cycle.

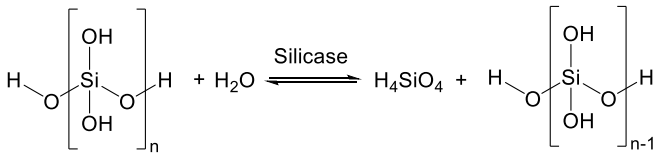

Scheme 2. Reaction catalyzed by SdoCA silicase.

and pathogens [15]. Natural silica production occurs on a massive scale annually, surpassing the production of silica by the entire chemical industry. From a chemical perspective, the high stability of siloxane bonds (≡Si-O-Si≡) results in accelerated silica dissolution only in alkaline pH regions by hydroxide ions (HO^-) and in acidic conditions by hydrogen ions (H^+) and fluoride ions (F^-) [16,17].

The breakdown of silicate biominerals, otherwise insoluble, by silicase profoundly influences the availability of silicates in the environment and dynamic of ecosystems. This enzyme was first isolated from the demosponge *Suberites domuncula* by W.E.G. Müller and colleagues, and it was proposed as analogous of a type *alpha* carbonic anhydrase (abbreviated as CA, EC 4.2.1.1) [6,18]. The CA is known as one of the "fastest enzymes", under certain conditions, and catalyzes the reversible hydration of carbon dioxide to carbonic acid, with a turnover number (k_{cat}) in the range of hundreds of thousands to millions of reactions per second [19,20]. The general reaction catalyzed by the silicase is described in Scheme 2.

Unlike CA, silicase exhibits lower catalytic activity than its counterpart enzyme [6]. Furthermore, research on its structure, catalytic mechanism, and other biochemical details remains limited, with very few publications addressing these aspects at present [6]. In addition, few patents reference these studies on the use of *alpha* and *gamma* type CA enzymes with silicase activity, exemplified by U.S. Patent No. 8822188B2, issued in 2014. Understanding the mechanisms and implications of silicase activity contributes to broader insights into ecosystem functioning and Earth's geochemical cycles, highlighting the intricate interplay between biological processes and environmental dynamics.

This study aims to provide a comprehensive understanding of silicase, exploring its kinetic profile, esterase activity, inhibition, and activation profile. We elucidate the evolutionary relationship between silicase and other related enzymes, shedding light on its potential functional roles in biological systems [21]. We gained insight into its esterase activity and compared it to human CA II (hCA II). Exploring the significance of silicon and mechanisms of biosilica formation in plants underscores their critical role in enhancing plant growth and resilience to diseases and stressors [2,22]. Therefore, we examined its inhibition and activation profile with respect to a series of aromatic or heterocyclic sulfonamides (as inhibitors) and amines/amino acids (as activators) known for hCA II [23]. Finally, to gain insights into the biochemical mechanism of silicase, we have explored its three-dimensional model computationally.

As final note, it is intriguing to observe that the counterpart enzyme responsible for catalyzing the hydrolysis and condensation of orthosilicic acid (H_4SiO_4 or $Si(OH)_4$) into silica (SiO_2), known as silicatein, shares a remarkable similarity with serine proteases such as trypsin and chymotrypsin, which are significant types of proteases functioning as a general acid-base catalyst at neutral pH [24–26]. Hence, it appears that nature leverages enzymatic expertise both in the production and breakdown of silica-based materials through silicase.

2. Materials and methods

2.1. Construction of expression plasmids

The synthetic silicase gene (abbreviated as SdoCA) was designed in our labs and produced by Life Technologies (Invitrogen, Carlsbad, CA), which specializes in gene synthesis. The SdoCA gene (GenBank accession DD298191; residues aa96-aa379) contained *Nde*I and *Xho*I restriction sites at the 5′- and 3′-ends, respectively, and four base-pair sequences (CACC) necessary for directional cloning at the corresponding 5′-end of the silicase gene. The synthetic SdoCA was ligated into the expression vector pET100/D-TOPO (Invitrogen, Carlsbad, CA) to form the expression vector pET100D-Topo/SdoCA, containing a nucleotide sequence encoding for a polypeptide with an additional six histidine residues before the insertion point to facilitate the purification of the target protein. The integrity of the SdoCA gene and absence of errors in the ligation sites were confirmed by bidirectional automated sequencing.

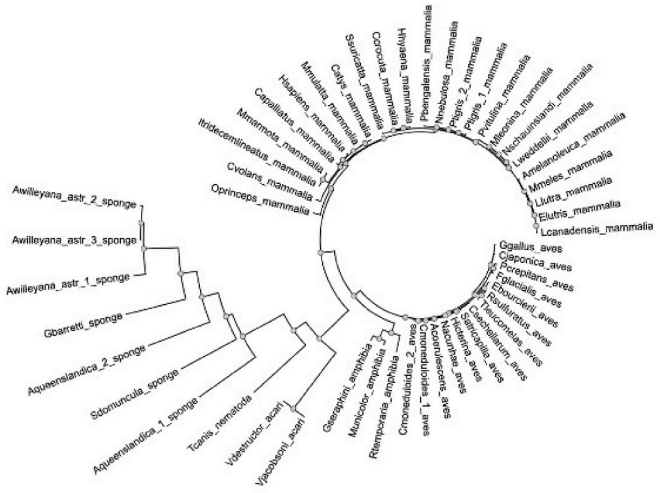

Fig. 1. Dendrogram illustrating the phylogenetic analysis of silicase sponges alongside CAs from diverse taxa.

2.2. Bacterial strains and materials

Escherichia coli DH5a cells (Agilent, USA) were used for initial cloning, while *E. coli* BL21 (DE3) cells (Agilent, Santa Clara, CA, USA) were utilized for the heterologous expression of the recombinant SdoCA. The pET100/D-TOPO vector was purchased from Invitrogen (Carlsbad, CA) with the feature to express the recombinant protein as a fusion protein with a 6-histidine tag at the N-terminus. Luria Bertani Broth (LB), ampicillin, and other chemicals were obtained from Merck (Darmstadt, Germany).

2.3. Sequence analysis and molecular modeling

The silicase sequence encoded by the *S. domuncula* genome (abbreviated as SdoCA) was analyzed using BLAST and compared with a database of proteins from various species. The dendrogram was built using PhyML 3.0 [27]. Protein modeling was performed using AlphaFold under the website resource ColabFold v1.5.5: AlphaFold2 using MMseqs2 [28]. The quality of generated models was inferred from predicted per-residue confidence scores or pDDLT (0–100). The SdoCA was compared to the experimental model of the atomic resolution of hCA II (PDB accession code 3ks3 [29]) was used. Theoretical molecular weight of SdoCA was predicted from amino acid composition using ProtParam tool (https://web.expasy.org/protparam/) from Expasy bioinformatic resource.

2.4. Expression and purification of SdoCA

Competent *E. coli* BL21 (DE3) (Agilent, Santa Clara, CA, USA) cells were transformed with pET100D-Topo/SdoCA. A single colony of transformed *E. coli* BL21 (DE3) was incubated overnight on a shaking incubator in 10 mL Luria-Bertani broth (LB) medium containing ampicillin (100 mg/mL), at 37 °C with constant agitation (200 rpm). The next day, 5 mL of cultured materials was removed and inoculated in 1 L of LB broth. The culture was grown until an OD600nm value of 0.6 was reached under vigorous shaking (200 rpm), at 37 °C. Isopropyl-b-D-thiogalactopyranoside (IPTG) was added to a final concentration of 1 mM, and 0.5 mM $ZnSO_4$ was added after 30 min incubation for uptake in the expressed protein. The incubation period continued for an additional 3 h at 37 °C with shaking at 200 rpm. Then, the bacterial suspension was tested and analyzed on 12 % SDS-PAGE to verify the overexpression of SdoCA. Sodium dodecyl sulfate SDS-polyacrylamide gel electrophoresis (SDS-PAGE) was performed as described by Laemmli using a 12 % gel [30]. Purification was performed by using standard Ni-column chromatography.

2.5. Enzymatic assays

A stock solution of SdoCA (MW 36.9 KDa) with concentration of 0.7 mg/mL, in buffer Tris-HCl 50 mM pH 8.3, 150 mM NaCl, 10 % w/v glycerol was used for the enzymatic assay. An Applied Photophysics stopped-flow instrument was used to assay the CA catalyzed CO_2 hydration activity [31]. Phenol red (at a concentration of 0.2 mM) was used as an indicator, working at the absorbance maximum of 557 nm, with 20 mM Hepes (pH 7.4) as a buffer, and 20 mM Na_2SO_4 (to maintain constant ionic strength), following the initial rates of the CA-catalyzed CO_2 hydration reaction for a period of 10–100 s. The CO_2 concentrations ranged from 1.7 to 17 mM for the determination of the kinetic parameters and inhibition constants [23]. Enzyme concentration used was 12.6 nM. For each modulator, at least six traces of the initial 5–10 % of the reaction were used to determine the initial velocity. The uncatalyzed rates were determined in the same manner and subtracted from the total observed rates. Stock solutions of the modulator (0.1 mM) were prepared in distilled–deionized water and dilutions up to 0.01 nM were done thereafter with the assay buffer. Modulator and enzyme solutions were preincubated together for 15 min at room temperature prior to the assay, to allow for the formation of the E-I complex. The inhibition constants were obtained by non-linear least-squares methods using PRISM 3 and the Cheng-Prusoff equation and represent the mean from at least three different determinations [32].

2.6. Silicase assay

A saturated solution was prepared by mixing 30 mg/L of silica in buffer (20 mM Hepes (pH 7.4) and 20 mM Na_2SO_4) A total of 1 mL was obtained by mixing 810 μL with of saturated silica solution with 190 μL SdoCA stock solution with concentration of 0.7 mg/mL. The biochemical reaction was kept for 16 h at room temperature in order to allow the silica breakdown and solubilization. The amount of released silicic acid (H_4SiO_4) was evaluated through a silicon test [33]. Calibration curve was built using $Na_2SiO_3{\cdot}5H_2O$ 1 M and dilutions in the same buffer solution.

2.7. Esterase assay

Considering the SdoCA's capability to cleave a Si-ester bond (-O-Si-), we conducted an esterase assay targeting a similar esterase R-COO-R′ bond breakdown. The substrate employed was the same as that utilized for testing hCA II esterase: 4-nitrophenyl acetate (PNA). In all cases, the reaction was initiated by adding the substrate (1 mM of PNA), and the enzyme activity at different concentrations was measured by monitoring the production of colored product, 4-nitrophenol (4-NP), at 400 nm every 2 min for about 2 h at room temperature. In all cases, before calculating the percentage of enzyme activity, absorbance of the spontaneous hydrolysis of the substrate was subtracted from esterase activity.

3. Results

3.1. Recombinant SdoCA

The SdoCA enzyme was expressed as a soluble construct corresponding to the 282 residues catalytic domain of silicase with a theoretical MW of 36.9 KDa, as reported by Schröer et al. [6]. The N-terminal region comprised a 6-His tail and a linker incorporating the enterokinase (EK) recognition site for eventual removal of the tag after protein purification. The SdoCA enzyme was expressed in *E. coli*, yielding approximately 5 mg of protein from 3.3 g of cell paste. Upon nickel column, the purity of the protein preparation was 85–90 % on the base of SDS-PAGE (Fig. S1).

Table 1
Kinetic parameters for the CO_2 hydration reaction catalyzed by the human cytosolic isozymes hCA I and II (α-class CAs) and *S. domuncula* SdoCA at 20 °C and pH 7.4 in 20 mM HEPES buffer.

Organism	Enzyme Acronym	Class	k_{cat} (s^{-1})	K_M (mM)	k_{cat}/K_M (M^{-1} s^{-1})	K_I (AAZ) (nM)
Homo sapiens	hCA I	α	2.0 x 10^5	4.0	5.0 x 10^7	250
	hCA II	α	1.4 x 10^6	9.3	1.5 x 10^8	12
S. domuncula	SdoCA	α	1.43 x 10^5	2.6	5.5 x 10^7	891

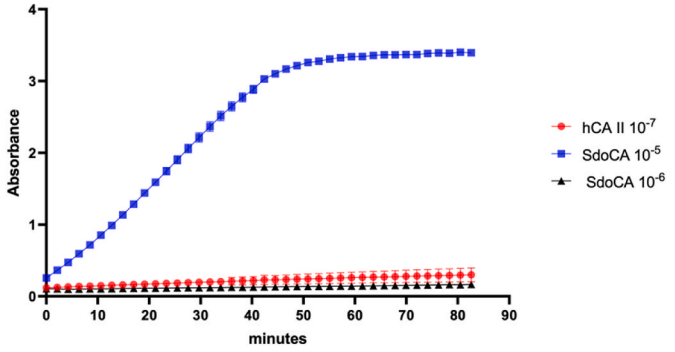

Fig. 2. Esterase reaction by SdoCA and hCA II. Spectrophotometric measurement of *p*-nitrophenol release as result of esterase C-O bond cleavage by SdoCA as compared with hCA II. Enzymes molar concentration used for the assay are indicated. The curves have been corrected by the spontaneous hydrolysis of the substrate *p*-nitrophenyl acetate under comparable conditions.

Table 2
Silicic acid production through silicase assay. This assay quantifies free silicic acid released from amorphous silica using the colorimetric "silicon test" that measures the absorbance of the released adduct with silicic acid at 810 nm [33].

Enzyme digestion (16h)	Absorbance		Equivalent in μg
	Average[a]	SD	
Silica solution (no enzyme)	0.0631	0.000666	12.36
Silica solution with hCA II (30 μg/mL)	0.0671	0.00512	13.14
Silica solution with SdoCA (37 μg/mL)	0.0946	0.006124	1364.24

[a] From 3 different assays.

3.2. Evolutionary analysis

As previously mentioned, SdoCA, along with silicases from various sponge organisms, exhibits similarities with various ***α***-CAs class across a range of taxa, including mammals, birds, amphibians, acari, and nematodes. These similarities are evident in key alignment metrics, as indicated by the maximum score values reported in Table S1. The multialignment across species, obtained using BLAST as shown in Fig. S2, includes all sequences reported in Table S1, offering insights into the evolutionary relationships and functional conservation among these groups of CAs. These enzymes are widely conserved across evolution and play crucial roles in diverse physiological processes. SdoCA shares some amino acid regions with ***α***-CAs from other species, suggesting a potential overlap in their biological functions (Fig. S2). Therefore, it is plausible to hypothesize that SdoCA may perform functions similar to those of CAs.

To deepen our understanding of the functional roles and evolutionary history between SdoCA and ***α***-CAs, we conducted a phylogenetic analysis, as described in the dendrogram (see Fig. 1).

This analysis reveals that sponge silicases, including SdoCA, form a distinct group separate from others, indicating a close and diversified evolutionary history compared to other taxonomic groups included in the analysis. Their unique positions in the phylogenetic tree suggest that sponge silicases have evolved uniquely from other taxa, such as mammals and birds, implying significant phylogenetic divergence over time. In addition, within the same silicase enzymes significant variation can be seen with exception of the minimal conservative residues among all the ***α***-CAs. These findings offer a fresh perspective on the evolutionary relationship between SdoCA and other ***α***-CAs across diverse taxa.

3.3. Kinetic measurements and silicase activity

Consistently with this phylogenetic analysis, the kinetic measurements show a promiscuity of SdoCA towards different substrates. Notably, the enzyme exhibits a K_M value of 2.6 mM for anhydrase activity (CO_2 hydration activity) at pH 7.4 in Tris-HCl buffer, as shown in Table 1. This reaction consists in the catalysis of the reversable hydration reaction of carbon dioxide: $CO_2 + H_2O \Leftrightarrow HCO_3^- + H^+$ and is catalyzed by known class α-CA isozymes in mammals including hCA I and hCA II, the prototypical carbonic anhydrase isozyme, containing a zinc ion tetrahedrally coordinated to three-canonical histidine residues [20]. In comparison to SdoCA (K_M value of 2.6 mM), and as expected, hCA I and hCA II exhibits a higher K_M value of 4.0 and 9.3 mM for anhydrase activity, respectively, and under same conditions. Interestingly, SdoCA exhibits k_{cat}/k_M of 5.5 x 10^7 M^{-1} s^{-1} similar to the CAs, used as control, hCA I and about one order magnitude lower than hCA II, which operates near the limit of diffusion control with a k_{cat}/K_M (M^{-1} s^{-1}) of 1.5 x 10^8 M^{-1} s^{-1} (Table 1). Thus, SdoCA does display a significant anhydrase activity.

Similarly, the release of 4-nitrophenol (4-NP), resulted from the esterase-mediated cleavage of the C-O bond by SdoCA, is measured spectrophotometrically as shown in Fig. 2.

Specifically, the production of the colored product, 4-NP, was observed at 400 nm, indicating significant C-O bond cleavage activity by SdoCA at the concentration of 10^{-5} M. Conversely, when the concentration was decreased by an order of magnitude, the esterase activity decreased drastically, resulting in significantly lower activity compared to hCA II at the concentration of 10^{-7} M.

Table 3
Inhibition of SdoCA and hCA II by anion molecules as obtained by a stopped-flow CO_2 hydrase assay [31].

K_I (mM)[a]					
Cmp	SdoCA	hCAII	Cmp	SdoCA	hCAII
NO_2^-	>100	>100	**ClO_4^-**	33.2	>100
NO_3^-	>100	95.5	**SnO_3^{2-}**	31.8	6.0
HCO_3^-	84.6	>100	**SeO_4^{2-}**	25.6	0.70
CO_3^{2-}	82.1	82.5	**TeO_4^{2-}**	22.0	60.5
HSO_3^-	>100	3.7	**OsO_5^{2-}**	>100	0.95
SO_4^{2-}	>100	>100	**$P_2O_7^{2-}$**	>100	0.8
F^-	>100	>100	**$V_2O_7^{2-}$**	>100	2.7
Cl^-	76.8	>100	**$B_4O_7^{2-}$**	>100	1.0
Br^-	>100	>100	**ReO_4^-**	>100	4.4
I^-	92.6	>100	**RuO_4^-**	>100	4.9
CNO^-	23.8	37.0	**$S_2O_8^{2-}$**	>100	0.061
SCN^-	76.0	9.3	**$SeCN^-$**	91.4	32.5
HS^-	>100	7.2	**$NH(SO_3)^{2-}$**	41.9	13.7
CN^-	>100	61.8	**FSO_3^-**	>100	>100
N_3^-	9.2	89.2	**CS_3^{2-}**	64.0	0.07
Sulfamide	0.14	49.2	**Et_2NCS^{2-}**	>100	0.50
Sulfamic Acid	>100	25.2	**PF_6^-**	>100	1.7
Ph-B(OH)$_2$	>100	0.90	**Triflate**	>100	5.5
Ph-AsO_3H_2	>100	67.1			

[a] Mean from 3 different assays, by a stopped flow technique (errors were in the range of ± 5–10 % of the reported values).

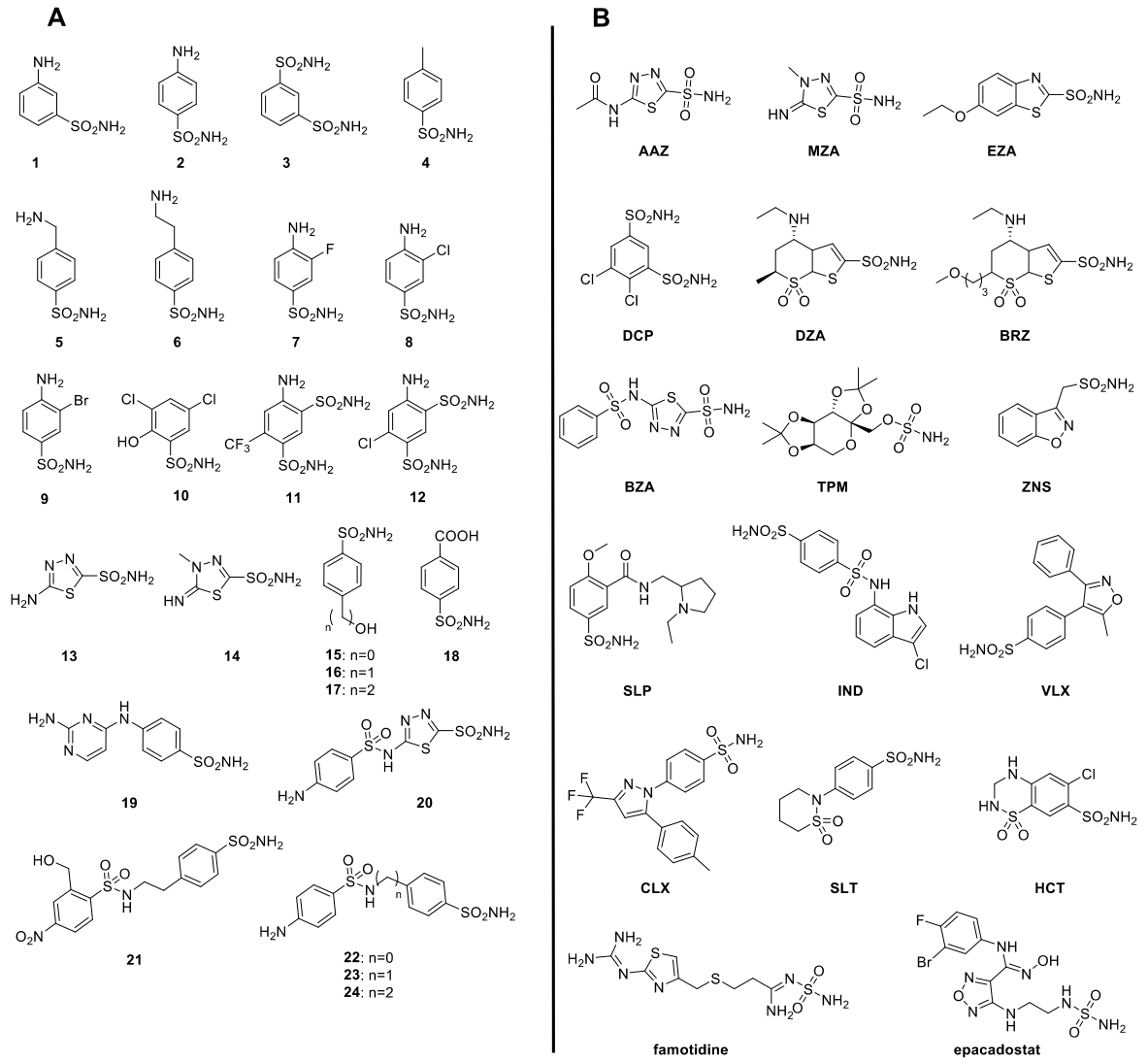

Fig. 3. A. Molecular structures of selective CAIs including sulfonamides and their bioisosteres. **B.** Molecular structures of **AAZ-EPA** series of clinically employed for the management and treatment of various diseases and tested for inhibition of SdoCA.

Then, we assessed silicase activity of recombinant SdoCA by using a mixture containing 30 mg/mL of amorphous silica in a buffer solution at pH 7.4 as the substrate. Following the addition of the recombinant enzyme, the reaction was allowed to proceed for 16 h at a temperature of 25 °C. The production of silicic acid was quantified through absorbance measurements at 810 nm with the "silicon test", leveraging a calibration curve (shown in Fig. S3) [33]. The activity assay demonstrated that SdoCA effectively catalyzes the depolymerization of amorphous silica and a quantitative analysis revealed that a concentration of 37 μg of the recombinant enzyme released 1.4 mg of free silicic acid, as reported in Table 2. The hCA II enzyme displays no significant silicase activity as compared to SdoCA (see Table 2).

3.4. Silicase modulation by CAIs and CAAs

Moreover, we assessed the impact of various compounds, including CA inhibitors (CAIs) and activators (CAAs), on silicase enzymatic activity. One rationale for utilizing CAIs and CAAs is their potential to interact with silicase due to structural or functional similarities between CA and silicase enzymes. Furthermore, investigating the effects of CAIs and CAAs on silicase activity could yield valuable insights into potential cross-talk or interplay among different metabolic pathways involved in plant silicon metabolism, deepening our understanding of its mechanism of action and identifying potential candidates for the development of biotechnological tools or molecules capable of influencing silicon metabolism in plants and diatoms.

We investigated a wide range of inorganic and organic anions, as well as closely related with a geometry similar to small molecules including SdoCA product reaction known for their interactions with metal ions in the active sites of CAs [34] (see Table 3). These interactions primarily entail coordinating the metal ion at the enzyme's active site, often through monodentate ligand formation that preserves the tetrahedral geometry of the metal ion. However, occasionally, trigonal bipyramidal geometries are observed, particularly relevant to the zinc ion found in various classes of CAs [35].

The information outlined in Table 3 provides inhibition profiles for SdoCA and hCA II by various anions, elucidating the inhibition characteristics of the silicase enzyme in comparison to the hCA II, thus enabling a direct comparison:

1. Carbonate and bicarbonate anions were found to exhibit low inhibition potency towards SdoCA, mirroring their effects on hCA II. Similarly, no inhibition was observed with nitrate, nitrite, fluoride, and bromide anions.

Table 4
Inhibition profile of SdoCA and hCA II by thirty-eight sulfonamide, one sulfamate, and two sulfamide derivatives by a stopped-flow CO_2 hydrase assay [31].

K_I (nM)[a]					
Cmp	SdoCA	hCAII	Cmp	SdoCA	hCAII
1	826.6	300	**22**	891.8	46
2	2284	240	**23**	1431	33
3	2798	8	**24**	1702	30
4	705.9	320	**AAZ**	891.5	12
5	2249	170	**MZA**	3953	14
6	1950	160	**EZA**	3471	8
7	1590	60	**DZA**	875.1	9
8	1754	110	**BRZ**	8571	3
9	1526	40	**BZA**	8208	9
10	2250	54	**TPM**	3798	10
11	501.9	63	**SLP**	667.4	40
12	725.8	75	**IND**	6060	15
13	86.8	60	**ZNS**	3532	35
14	86.1	19	**CLX**	7858	21
15	95.9	80	**VLX**	4634	43
16	555.5	94	**SLT**	2289	9
17	93.4	125	**SAC**	7041	5959
18	572.5	46	**HCT**	1230	290
19	271.0	33	**DCP**	4873	38
20	170.7	2	**FAM**	4916	58
21	253.7	11	**EPA**	5963	917

[a] Mean value from 3 different assays, by a stopped flow technique (errors were in the range of ± 5–10 % of the reported values).

2. Moderate inhibition of SdoCA was observed using chloride, iodide, carbon trisulfide, and the seleno and thiocyanate anions, resulting in inhibition constants (K_{Is}) in the range 64.0–92.6 mM.
3. Azide anion displayed significant inhibition against SdoCA, with a K_I of 9.2 mM.
4. The most potent inhibitor of SdoCA was identified as sulfamide, showing a K_I of 0.14 mM. Several crystallographic studies for the human CAs have revealed coordination to the catalytic zinc ion [36]. Notably, as compared to hCA II, sulfamide showed over 350-fold higher inhibitory activity against SdoCA indicating a promising lead compound for designing potent SdoCA inhibitors.

Following the insights garnered from sulfamide inhibition, our focus shifted towards evaluating SdoCA interaction to an array of sulfonamides and their bioisosteres. The molecular structures of compounds **1–24**, shown in Fig. 3A, range from simple aromatic to heterocyclic sulfonamides that are often utilized as building blocks for developing novel, potent, and selective CAIs [37,38]. Additionally, the series **AAZ-EPA** (acetazolamide-ethoxzolamide), reported in Fig. 3B, are clinically employed for the management and treatment of various diseases, including glaucoma, idiopathic intracranial hypertension, altitude sickness, congestive heart failure, epilepsy, among others [39–41].

The following results can be observed from the bioisosteres inhibition data reported in Table 4:

1. The aromatic sulfonamide compounds **1–12** exhibited weak inhibition against SdoCA, with K_I values ranging from the high nanomolar to the micromolar (501.9–2250 nM). Notably, the sulfonamide moiety in position *meta* to the aromatic core was less active compared to compound **1**, which has the sulfonamide in *para* position. This difference in activity highlights a notable disparity in inhibition efficacy compared to hCA II for these derivatives. Conversely, the thiadiazole core found in derivatives **13** and **14** demonstrated significantly higher inhibitory potency, with K_I values of 86.8 and 86.1 nM, respectively. For derivatives **15–17**, an interesting observation was the critical role of the OH chain length in modulating inhibitory activity; specifically, phenolic sulfonamide **15** showed a K_I of 95.9 nM, whereas the introduction of a benzyl alcohol group in compound **16** resulted in a nearly six-fold decrease in activity. Compounds **18–24**, characterized by more complex tail structures, exhibited moderate inhibition of SdoCA, with K_I values ranging from 170.7 nM to 891.8 nM.
2. In the case of the **AAZ-EPA** series, all derivatives demonstrated weak inhibitory activity in the micromolar range (1230 nM–8571 nM), with the exceptions of **AAZ** and **DZA** (Dorzolamide**)**, which had K_I values of 891.5 nM and 875.1 nM, respectively.
3. Table 4 shows a distinct inhibition pattern for the silicase enzyme compared to human hCA II, highlighting the thiadiazole scaffold as a particularly effective chemical structure for developing potent inhibitors against this specific isoform.

Next, we explored the activation potential of a panel of amino acid and amine derivatives 1–24 on SdoCA. These compounds have previously been identified as CAAs effective across all known genetic CA families, according to existing kinetic and crystallographic evidence [42]. Amino acids and amines **1**–**24** investigated as CAAs are shown in Fig. 4 and have been tested with SdoCA.

This evidence suggests that the activators bind to a distinct region within the enzyme active site, separate from where substrate binding occurs [43,44]. Consequently, these activators do not alter the Michaelis constant (K_M) but specifically enhance the catalytic constant (k_{cat}). Our investigation into activators **1**–**24** aimed to elucidate their efficacy in activating SdoCA and to delineate their structure-activity relationship (SAR) profiles. Activation constants for these compounds were measured against SdoCA and hCA II, providing a basis for comparative analysis as reported in Table 5.

The key findings for SdoCA activation by SAR compounds can be summarized as following:

1. The *L*- and *D*-isomers of amino acids show significant differences in their inhibitory activity towards SdoCA, indicating that the stereochemistry of these molecules greatly influences enzyme binding and activation. Notably, *L*-His exhibits a much stronger SdoCA activation (0.66 μM) compared to its *D*-form (8.65 μM) as well as for the case of *L*-Tyr that was more active than *D*-Tyr. Whereas *D*-Phe showed more potent SdoCA activation (17.66 μM) than its *L*-counterpart (>100 μM), highlighting the enzyme stereo-selective preferences.
2. Biogenic amines such as serotonin and histamine showed more potent activation towards SdoCA (4.34 μM and 6.15 μM, respectively) compared to hCA II (50 μM and 125 μM, respectively) suggesting specific interactions favouring the SdoCA activation that could be attributed to differences in the active site structure. *L*-Asp with K_A values of >100 μM for SdoCA and hCA II indicating ita lack of effective activation with both enzyme isoforms active sites.

3.5. Structural modeling analysis

To gain structural insight into the similarities and differences between SdoCA and hCA II, correlating with the observed kinetic processing of various substrates, we analyzed the best AlphaFold model of SdoCA. The model comprises a total of 379 residues and scores with a pLDDT of 72.1 and a pTM of 0.667, as obtained from computational analysis. The PAE plot, a predicted aligned error for multimer structure predictions and crosslinks for the best model was generated using PAE Viewer (see Fig. S4) [45]. The best model is labeled as *rank_001_alphafold2_ptm_model_4_seed_000*). The comparison between SdoCA model and the hCA II (hCA II, pdb ID 3ks3) shows a similar superimposed core (showed in Fig. 5A, corresponding to silicase and residues 92-339), despite an amino sequence identity of 34.0 % (238 residues).

The superposition of silicase SdoCA and hCA II structural models exhibits a root-mean-square (r.m.s.) deviation of 0.85 Å for 183 pruned C-alpha atom pairs corresponding to silicase SdoCA residues 92–339. Similar considerations can be drawn by comparing the structural model of SdoCA and hCA V (as shown in Fig. 5B). The structural comparison of the two models reveals that the segment Y88-Q136 in hCA V is shorter in

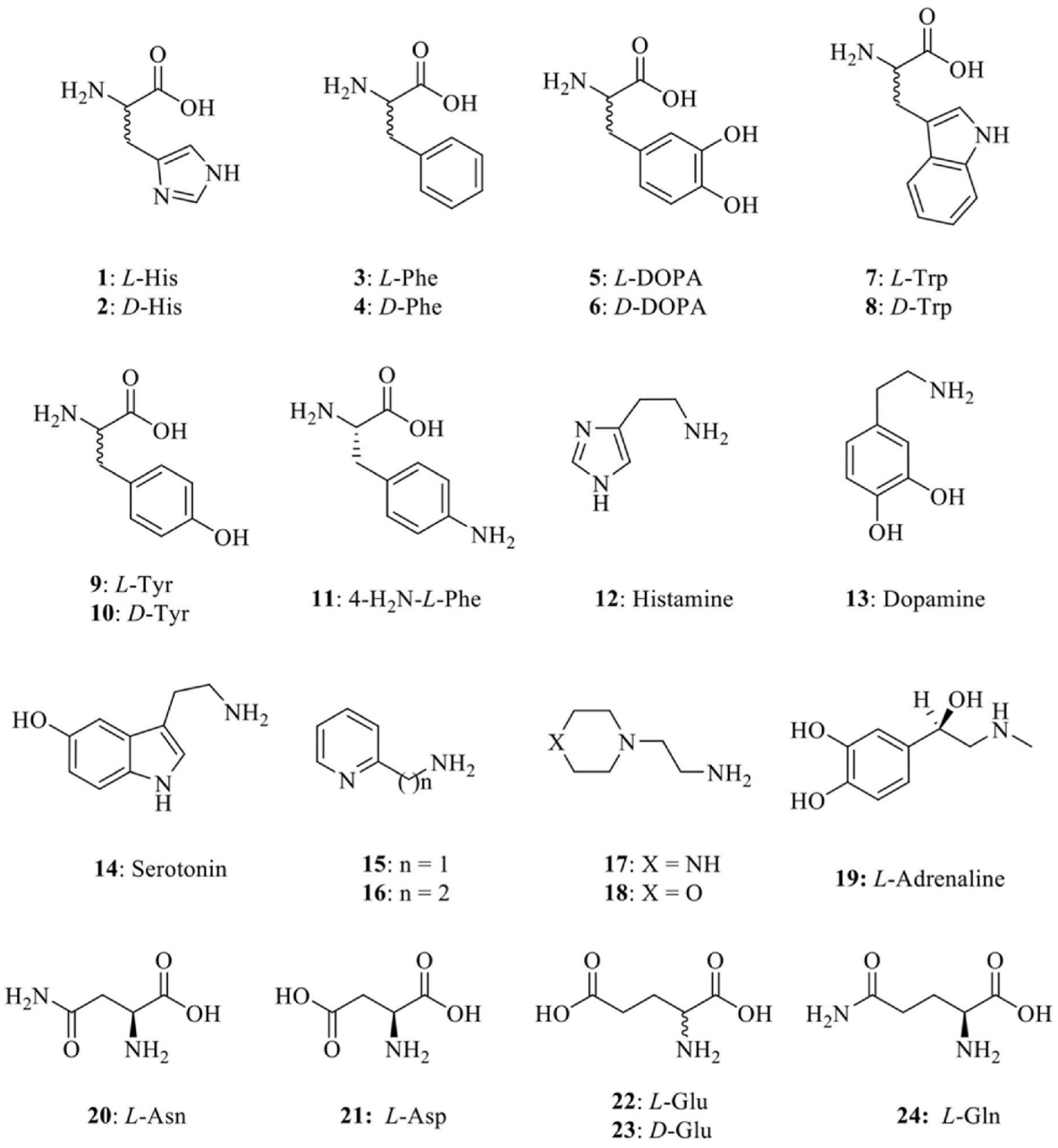

Fig. 4. Molecular structures of amino acid and amine derivatives identified as CAAs.

SdoCA (residues K122-A133) thus allowing to a larger cleft, considering the polymeric nature of the silicate substrate (Fig. 5B). Along with these details, the comparison of the Coulomb surfaces between SdoCA and hCA II reveals an increased region negative charge around D178 (see Fig. 6).

SdoCA, as analyzed by PocketMiner, a graph neural network trained to predict the likely locations of pocket openings (as shown in Fig. S5), revealed an intriguing finding: despite similarities, there was a slightly higher "cryptic pocket" score compared to hCA II [48].

Regarding the biochemical mechanism of the canonical hCA II for the interconversion of CO_2 and HCO_3^- (see Fig. 7A), it involves the generation of a zinc-bound hydroxide ion through a series of proton transfer steps, including the participation of a histidine residue (H64) acting as a proton shuttle [49,50].

Instead, the structural model of SdoCA reveals the presence of a Y64 residue in place of the H64 in hCA II [51]. This aromatic residue is equivalent to the Y64 found in hCA V, which in turn also displays an anhydrase activity of about 20 times less in comparison to hCA II [46]. Interestingly, in SdoCA Y64 is followed by residue Y65 which in turn is located within 5 Å of the zinc ion, while in hCA V, the equivalent residue to Y65, is represented by F65 [46]. In crystal structure of hCA V in complex with the transition state analogue acetazolamide, the nearest residue to the zinc ion associated with a key role in the catalytic activity is Y131, which differs from our studied SdoCA where Y65 near the zinc ion is present instead [46]. The vicinal residues Y64-Y65 SdoCA to the coordinated zinc ion suggests their participation to the proton wire for proton transfer shuffling for generating the nucleophile HO^- necessary for catalytic activity. This wire could be the equivalent of E62/E84 in gamma-CA from *M. Thermophila* or the proton wire of water molecules found in the double mutant F65A/Y131C-methylimidazole of CAV [49,52]. In the 3D model of SdoCA, a network of aligned hydrogen-bonded residues (H92, D91, and K124) is observed, as shown in Fig. 5B. Specifically, residue D91 (using the numbering equivalent to hCA II), presumably deprotonated, accepts a hydrogen bond from H90, which in

Table 5
Activation constants (K_A) of SdoCA and hCA II by amino acids and amines **1–24** determined by a stopped-flow CO_2 hydrase assay [31].

K_A (μM)[a]			
No.	Cmp	SdoCA	hCA II
1	***L*-His**	0.66	10.9
2	***D*-His**	8.65	43
3	***L*-Phe**	>100	0.013
4	***D*-Phe**	17.66	0.035
5	***l*-DOPA**	10.74	11.4
6	***d*-DOPA**	47.53	7.8
7	***L*-Trp**	11.13	27
8	***D*-Trp**	24.42	12
9	***L*-Tyr**	14.08	0.011
10	***D*-Tyr**	>100	0.013
11	**4-NH2-*L*-Phe**	16.93	0.15
12	**Histamine**	6.15	125
13	**Dopamine**	24.84	9.2
14	**Serotonin**	4.34	50
15	**2-Pyridyl-methylamine**	5.31	34
16	**2-(2-Aminoethyl)pyridine**	38.26	15
17	**1-(2-Aminoethyl)-piperazine**	22.86	2.3
18	**4-(2-Aminoethyl)-morpholine**	5.31	0.19
19	***l*-Adrenaline**	61.73	96
20	***L*-Asn**	14.25	>100
21	***L*-Asp**	>100	>100
22	***L*-Glu**	24.55	>100
23	***D*-Glu**	16.38	>100
24	***L*-Gln**	33.39	>50

[a] Mean from 3 different assays, by a stopped flow technique (errors were in the range of ± 5–10 % of the reported values).

turn donates a hydrogen bond to H94 coordinating the zinc ion required for catalysis. The residue D91 in SdoCA is oriented by a charge interaction with K124 (Fig. 5B). The linear arrangement of these residues, and its proximity to the entrance of the active site, suggests an optimal configuration for substrate orientation in the active site. Therefore, based on the structural considerations, we suggest a possible catalytic mechanism, as depicted in Fig. 7B.

4. Conclusion

In conclusion, our results demonstrate that SdoCAs, as ***α***-CAs have silica-related activities, expanding their catalytic roles beyond hydration. The active site and the other structural features of ***α***-CAs accommodate silica molecules or the anhydrase activity displayed by SdoCA, impacting pH and facilitating silicase activity. This additional function may have emerged due to evolutionary pressures or genetic mutations, conferring adaptive advantages in silica-rich environments. Such adaptations likely contributed to species survival and diversification through natural selection. Analyzing inhibitory and activating molecules provides valuable insights into the structure, dynamics, and active sites of the enzyme, as well as its interactions with substrates and modulators. Such insights can inform the design of more potent inhibitors or activators of silicase, thereby influencing plant or diatom performance under challenging environmental conditions.

CRediT authorship contribution statement

Andrea Angeli: Writing – review & editing, Visualization, Validation, Software, Methodology, Formal analysis, Data curation, Conceptualization. **Viviana De Luca:** Writing – review & editing, Validation, Software, Resources, Methodology, Formal analysis, Data curation. **Clemente Capasso:** Writing – review & editing, Visualization, Validation, Supervision, Software, Resources, Methodology, Investigation, Formal analysis, Data curation, Conceptualization. **Luigi F. Di Costanzo:** Writing – review & editing, Writing – original draft, Visualization, Validation, Supervision, Software, Methodology, Investigation, Formal analysis, Data curation, Conceptualization. **Claudiu T.**

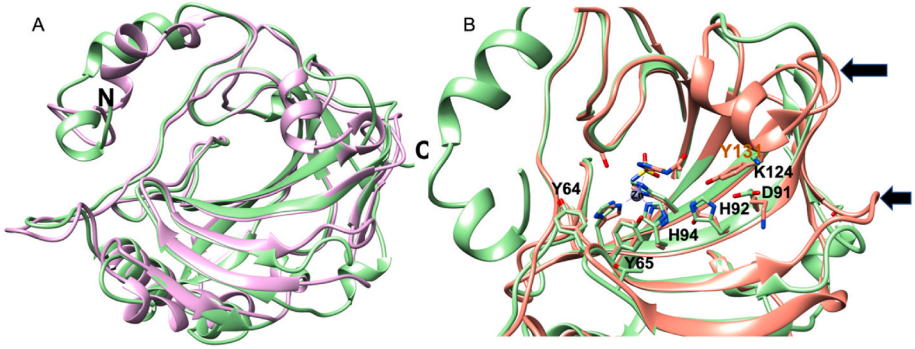

Fig. 5. A. Least-squares superposition of unliganded *S. domuncula* SdoCA (green, AlphaFold model, this work) and the crystal structure of Zn-hCA II complex (purple, pdb entry 3ks3). B. Active site displaying selected residues involved in zinc ion coordination and catalytic activity for SdoCA (green) and **the crystal structure of Zn-**hCA V in complex with the transition state analogue acetazolamide (orange, pdb entry 1dmy [46]). Differences between the SdoCA and hCA V models at the entrance of the active site are highlighted by black arrows.

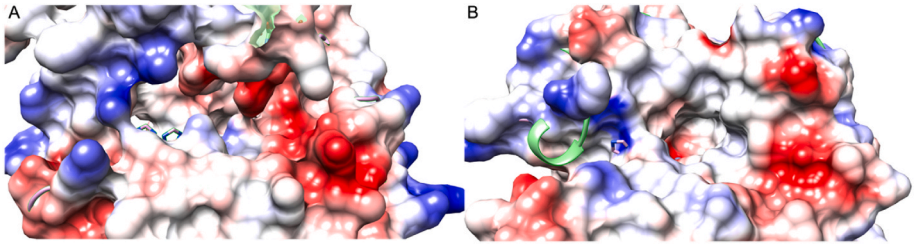

Fig. 6. Electrostatic surface potential of SdoCA (A) and hCA II (B) calculated with Chimera [47]; the color scale ranges from −10 kcal/mol*e$^-$ (red) to +10 kcal/mol*e$^-$ (blue). Note the more extensive negative electrostatic surface potential surrounding the region corresponding to D91 of SdoCA. This feature reflects the adaptation of the silicase for anchoring polymerized silica.

A

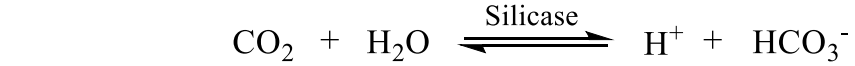

B

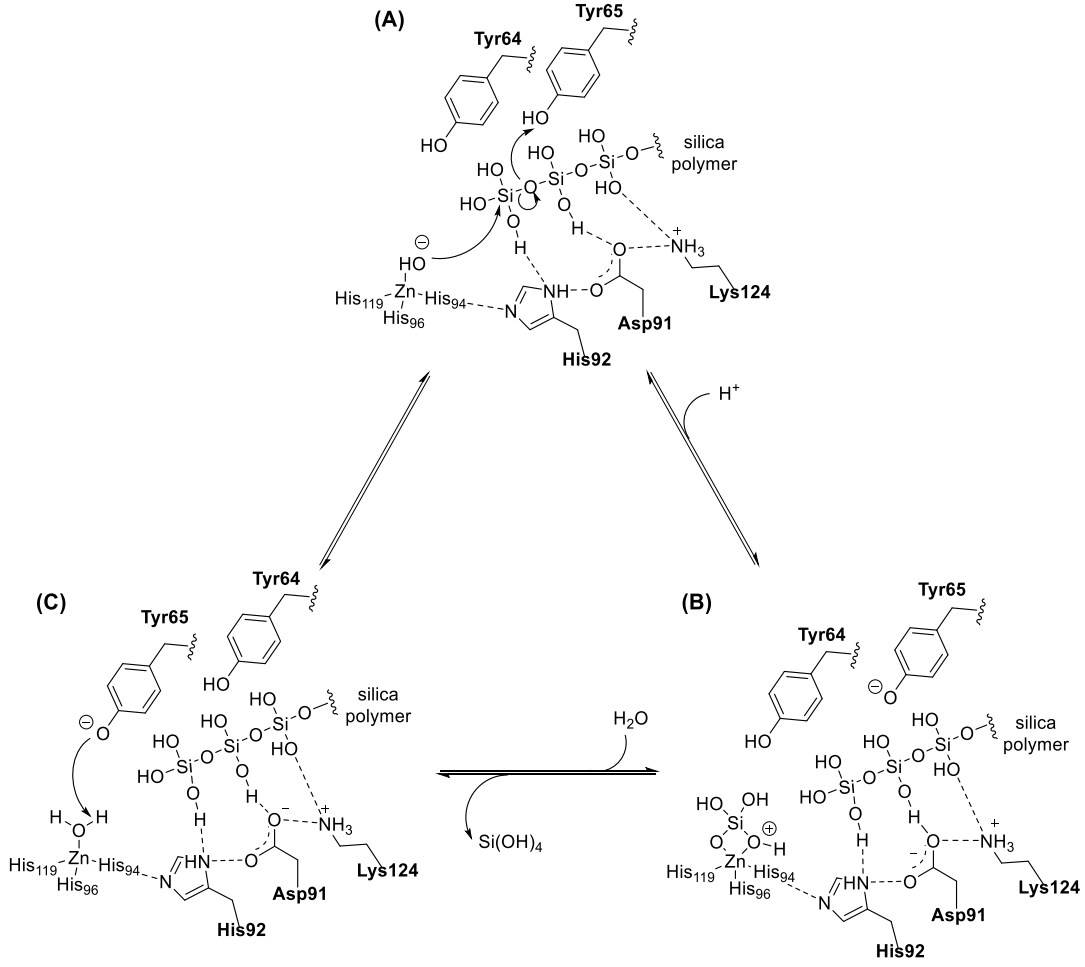

Fig. 7. A. Hydration reaction catalyzed by SdoCA. (B) Suggested mechanism of the SdoCA silicase reaction. New features revealed by the computational SdoCA three-dimensional model indicate that residue Y65, positioned close to the zinc ion, could act as a general base to abstract a proton from the zinc-coordinated water molecule. This residue follows Y64 and could, therefore, participate in a proton relay. A network of aligned, hydrogen-bonded residues (H92, D91, and K124) could facilitate the movement of polymerized silica towards hydrolysis. Upon cleavage and departure of silicic acid, another water molecule coordinates to the metal ion, thereby restarting the cycle. SdoCA residues numbering refers to the canonical hCA II isozyme, for clarity.

Supuran: Writing – review & editing, Visualization, Validation, Supervision, Software, Resources, Project administration, Methodology, Investigation, Formal analysis, Data curation, Conceptualization.

Data availability

Data will be made available on request.

ABBREVIATIONS

CA	Carbonic Anhydrase
CAIs	CA inhibitors
CAAs	activators
AAZ-EPA	(acetazolamide-ethoxzolamide)

Appendix A. Supplementary data

Supplementary data to this article can be found online at https://doi.org/10.1016/j.abb.2024.110074.

References

[1] K.F. Brandstadt, Inspired by nature: an exploration of biocatalyzed siloxane bond formation and cleavage, Curr. Opin. Biotechnol. 16 (2005).
[2] M. Sahebi, M.M. Hanafi, A. Siti Nor Akmar, M.Y. Rafii, P. Azizi, F.F. Tengoua, et al., Importance of Silicon and Mechanisms of Biosilica Formation in Plants, 2015, BioMed, Research International, 2015.
[3] M.J. Uriz, X. Turon, M.A. Becerro, Silica deposition in demosponges: spiculogenesis in crambe crambe, Cell Tissue Res. 301 (2) (2000).
[4] M.J. Uriz, X. Turon, M.A. Becerro, Silica Deposition in Demosponges, 2003.
[5] M.J. Uriz, X. Turon, M.A. Becerro, G. Agell, Siliceous spicules and skeleton frameworks in sponges: origin, diversity, ultrastructural patterns, and biological functions, Microsc. Res. Tech. 62 (4) (2003).
[6] H.C. Schröer, A. Krasko, G Le Pennec, T. Adell, M. Wiens, H. Hassanein, et al., Silicase, an Enzyme Which Degrades Biogenous Amorphous Silica: Contribution to the Metabolism of Silica Deposition in the Demosponge Suberites domuncula, 2003, pp. 249–268.
[7] C.C. Perry, T. Keeling-Tucker, Biosilicification: the role of the organic matrix in structure control, J. Biol. Inorg. Chem. 5 (2000).

[8] L.L. Taylor, J.R. Leake, J. Quirk, K. Hardy, S.A. Banwart, D.J. Beerling, Biological weathering and the long-term carbon cycle: integrating mycorrhizal evolution and function into the current paradigm, Geobiology 7 (2) (2009).
[9] J.J. Bell, F. Strano, M. Broadribb, G. Wood, B. Harris, A.C. Resende, et al., Sponge functional roles in a changing world, in: Advances in Marine Biology, 2023.
[10] M. Maldonado, M. López-Acosta, C. Sitjà, M. García-Puig, C. Galobart, G. Ercilla, et al., Sponge skeletons as an important sink of silicon in the global oceans, Nat. Geosci. 12 (10) (2019).
[11] P. Tréguer, C. Bowler, B. Moriceau, S. Dutkiewicz, M. Gehlen, O. Aumont, et al., Influence of diatom diversity on the ocean biological carbon pump, Nat. Geosci. 11 (2018).
[12] J. Wulff, Sponge Contributions to the Geology and Biology of Reefs: Past, Present, and Future, 2016.
[13] R.A. Berner, A.C. Lasaga, R.M. Garrels, The carbonate-silicate geochemical cycle and its effect on atmospheric carbon dioxide over the past 100 million years, Am. J. Sci. 283 (7) (1983).
[14] D.E. Penman, J.K. Caves Rugenstein, D.E. Ibarra, M.J. Winnick, Silicate weathering as a feedback and forcing in Earth's climate and carbon cycle, Earth Sci. Rev. 209 (2020).
[15] H.A. Currie, C.C. Perry, Silica in plants: biological, biochemical and chemical studies, Ann. Bot. 100 (7) (2007).
[16] B.M. Mitsyuk, Mechanism of silica dissolution and state of silicic acid in hydrothermal solutions, Theor. Exp. Chem. 19 (5) (1984).
[17] F.K. Crundwell, On the mechanism of the dissolution of quartz and silica in aqueous solutions, ACS Omega 2 (3) (2017).
[18] W.E.G. Müller, H. Schröder, A. Krasko, Decomposition and modification of silicate and silicone by silase and use of the reversible enzyme, US Pat 7 (229) (2007) 807.
[19] D. Keilin, T. Mann, Carbonic anhydrase. Purification and nature of the enzyme, Biochem. J. 34 (8–9) (1940).
[20] M. Aggarwal, C.D. Boone, B. Kondeti, R. McKenna, Structural annotation of human carbonic anhydrases, J. Enzym. Inhib. Med. Chem. 28 (2013).
[21] Costanzo LF. Di, Atomic details of biomineralization proteins inspiring protein design and reengineering for functional biominerals, Chemistry 4 (2022).
[22] M. Luyckx, J.F. Hausman, S. Lutts, G. Guerriero, Silicon and plants: current knowledge and technological perspectives, Front. Plant Sci. 8 (2017).
[23] C.T. Supuran, Carbonic anhydrases: novel therapeutic applications for inhibitors and activators, Nat. Rev. Drug Discov. 7 (2008).
[24] S. Görlich, A.J. Samuel, R.J. Best, R. Seidel, J. Vacelet, F.K. Leonarski, et al., Natural hybrid silica/protein superstructure at atomic resolution, Proc. Natl. Acad. Sci. U.S.A. 117 (49) (2020).
[25] K. Shimizu, J. Cha, G.D. Stucky, D.E. Morse, Silicatein α: cathepsin L-like protein in sponge biosilica, Proc. Natl. Acad. Sci. U.S.A. 95 (11) (1998).
[26] J.N. Cha, K. Shimizu, Y. Zhou, S.C. Christiansen, B.F. Chmelka, G.D. Stucky, et al., Silicatein filaments and subunits from a marine sponge direct the polymerization of silica and silicones in vitro, Proc. Natl. Acad. Sci. U.S.A. 96 (2) (1999).
[27] S. Guindon, J.F. Dufayard, V. Lefort, M. Anisimova, W. Hordijk, O. Gascuel, New algorithms and methods to estimate maximum-likelihood phylogenies: assessing the performance of PhyML 3.0, Syst. Biol. 59 (3) (2010).
[28] J. Jumper, R. Evans, A. Pritzel, T. Green, M. Figurnov, O. Ronneberger, et al., Highly accurate protein structure prediction with AlphaFold, Nature 596 (7873) (2021).
[29] B.S. Avvaru, C.U. Kim, K.H. Sippel, S.M. Gruner, M. Agbandje-McKenna, D. N. Silverman, et al., A short, strong hydrogen bond in the active site of human carbonic anhydrase II, Biochemistry 49 (2) (2010).
[30] U.K. Laemmli, Cleavage of structural proteins during the assembly of the head of bacteriophage T4, Nature 227 (5259) (1970).
[31] R.G. Khalifah, The carbon dioxide hydration activity of carbonic anhydrase. I. Stop-flow kinetic studies on the native human isoenzymes B and C, J. Biol. Chem. 246 (8) (1971).
[32] C. Yung-Chi, W.H. Prusoff, Relationship between the inhibition constant (KI) and the concentration of inhibitor which causes 50 per cent inhibition (I50) of an enzymatic reaction, Biochem. Pharmacol. 22 (23) (1973).
[33] P. Rimmelin-Maury, T. Moutin, B. Quéguiner, A new method for nanomolar determination of silicic acid in seawater, Anal. Chim. Acta 587 (2) (2007).
[34] Simone G. De, C.T. Supuran, (In)organic anions as carbonic anhydrase inhibitors, J. Inorg. Biochem. 111 (2012).
[35] C.T. Supuran, How many carbonic anhydrase inhibition mechanisms exist? Vol. 31, J. Enzym. Inhib. Med. Chem. 31 (3) (2016), 345–345.
[36] P.A. Boriack, D.W. Christianson, J. Kingery-Wood, G.M. Whitesides, Secondary interactions significantly removed from the sulfonamide binding pocket of carbonic anhydrase II influence inhibitor binding constants, J. Med. Chem. 38 (13) (1995).
[37] A. Angeli, V. Kartsev, A. Petrou, M. Pinteala, R.M. Vydzhak, S.Y. Panchishin, et al., New sulfanilamide derivatives incorporating heterocyclic carboxamide moieties as carbonic anhydrase inhibitors, Pharmaceuticals 14 (8) (2021).
[38] C. Capasso, C.T. Supuran, An overview of the selectivity and efficiency of the bacterial carbonic anhydrase inhibitors, Curr. Med. Chem. 22 (18) (2014).
[39] C.T. Supuran, Emerging role of carbonic anhydrase inhibitors, Clin. Sci. 135 (2021).
[40] A. Angeli, L. Micheli, R. Turnaturi, L. Pasquinucci, C. Parenti, V. Alterio, et al., Discovery of a novel series of potent carbonic anhydrase inhibitors with selective affinity for μ Opioid receptor for Safer and long-lasting analgesia, Eur. J. Med. Chem. 260 (2023).
[41] A. Angeli, M. Ferraroni, C. Granchi, F. Minutolo, X. Chen, P. Shriwas, et al., First-in-Class dual targeting compounds for the management of seizures in glucose transporter type 1 deficiency syndrome, J. Med. Chem. 66 (14) (2023).
[42] A. Angeli, E. Berrino, S. Carradori, C.T. Supuran, M. Cirri, F. Carta, et al., Amine- and amino acid-based compounds as carbonic anhydrase activators, Molecules 26 (2021).
[43] F. Briganti, S. Mangani, P. Orioli, A. Scozzafava, G. Vernaglione, C.T. Supuran, Carbonic anhydrase activators: X-ray crystallographic and spectroscopic investigations for the interaction of isozymes I and II with histamine, Biochemistry 36 (34) (1997).
[44] C. Temperini, A. Scozzafava, C. Supuran, Carbonic anhydrase activation and the drug design, Curr. Pharmaceut. Des. 14 (7) (2008).
[45] C. Elfmann, J. Stülke, PAE viewer: a webserver for the interactive visualization of the predicted aligned error for multimer structure predictions and crosslinks, Nucleic Acids Res. 51 (W1) (2023).
[46] P.A. Boriack-Sjodin, R.W. Heck, P.J. Laipis, D.N. Silverman, D.W. Christianson, Structure determination of murine mitochondrial carbonic anhydrase V at 2.45-Å resolution: implications for catalytic proton transfer and inhibitor design, Proc. Natl. Acad. Sci. U.S.A. 92 (24) (1995).
[47] E.F. Pettersen, T.D. Goddard, C.C. Huang, G.S. Couch, D.M. Greenblatt, E.C. Meng, et al., UCSF Chimera - a visualization system for exploratory research and analysis, J. Comput. Chem. 25 (13) (2004) 1605–1612.
[48] A. Meller, M. Ward, J. Borowsky, M. Kshirsagar, J.M. Lotthammer, F. Oviedo, et al., Predicting locations of cryptic pockets from single protein structures using the PocketMiner graph neural network, Nat. Commun. 14 (1) (2023).
[49] K.M. Jude, S.K. Wright, C. Tu, D.N. Silverman, R.E. Viola, D.W. Christianson, Crystal structure of F65A/Y131C-methylimidazole carbonic anhydrase V reveals architectural features of an engineered proton shuttle, Biochemistry 41 (8) (2002).
[50] R.L. Mikulski, D.N. Silverman, Proton transfer in catalysis and the role of proton shuttles in carbonic anhydrase, Biochim. Biophys. Acta Protein Proteonomics 1804 (2010).
[51] C. Tu, D.N. Silverman, C. Forsman, B.H. Jonsson, S. Lindskog, Role of histidine 64 in the catalytic mechanism of human carbonic anhydrase II studied with a site-specific mutant, Biochemistry 28 (19) (1989).
[52] T.M. Iverson, B.E. Alber, C. Kisker, J.G. Ferry, D.C. Rees, A closer look at the active site of γ-class carbonic anhydrases: high-resolution crystallographic studies of the carbonic anhydrase from methanosarcina thermophila, Biochemistry 39 (31) (2000).